Available online at www.sciencedirect.com
SCIENCE DIRECT®
Journal of Catalysis 220 (2003) 47–56
JOURNAL OF CATALYSIS
www.elsevier.com/locate/jcat

Surface WO_4 tetrahedron: the essence of the oxidative coupling of methane over M–W–Mn/SiO_2 catalysts

Shengfu Ji,[a,b,c] Tiancun Xiao,[b] Shuben Li,[a] Lingjun Chou,[a] Bing Zhang,[a] Chuanzhi Xu,[a] Ruiling Hou,[a] Andrew P.E. York,[b,1] and Malcolm L.H. Green [b,*]

[a] *State Key Laboratory for Oxo Synthesis and Selective Oxidation, Lanzhou Institute of Chemical Physics, Chinese Academy of Sciences, 342 Tianshui Road, Lanzhou 730000, China*

[b] *Wolfson Catalysis Centre, Inorganic Chemistry Laboratory, University of Oxford, South Parks Road, Oxford, OX1 3QR, UK*

[c] *The Key Laboratory of Science and Technology of Controllable Chemical Reactions, Ministry of Education, Beijing University of Chemical Technology, 15 Beisanhuan Dong Road, PO Box 35, Beijing 100029, China*

Received 27 January 2003; revised 27 May 2003; accepted 28 May 2003

Abstract

A series of M–W–Mn/SiO_2 catalysts (M = Li, Na, K, Ba, Ca, Fe, Co, Ni, and Al) have been prepared and their catalytic performance for the oxidative coupling of methane (OCM) was evaluated in a continuous-flow microreactor. The structural properties of the catalysts have been studied using X-ray photoelectron spectroscopy (XPS), laser Raman spectroscopy (LRS), X-ray diffraction (XRD), and Fourier transform infrared spectroscopy (FTIR). In the trimetallic catalysts studied, there was evidence for WO_4 tetrahedron on the surface in the Li–, Na–, and K–W–Mn/SiO_2 catalysts, which is mainly present in the subsurface of the Ba–W–Mn/SiO_2 catalyst. It appears that the WO_4 has a strong interaction with the α-cristobalite support and is stabilized in the Na– and K–W–Mn/SiO_2 catalysts. However, the WO_4 species appear to be less stable in Li– or Ba–W–Mn/SiO_2 catalysts, in which the support turns into quartz SiO_2 or amorphous SiO_2. The WO_4 tetrahedron on the catalyst surface appears to play an essential role in achieving high CH_4 conversion and high C_2 hydrocarbon selectivity in the OCM reaction. Calculations suggest that the WO_4 tetrahedron interacts with the CH_4, giving suitable geometry and energy matching with CH_4, and this may account for the high OCM activities.

Keywords: Oxidative coupling of methane; M–W–Mn/SiO_2 catalyst; WO_4 tetrahedron; WO_6 octahedron; Structure

1. Introduction

The Na–W–Mn/SiO_2 catalyst system was first reported by Li and his co-workers [1,2], and has been one of the most effective catalysts for the oxidative coupling of methane [3–5]. It has been extensively studied by the groups of Li [6–24], Lunsford [25–30], Lambert [31,32], and Abedini [33]. Li's group proposed that W–O–Si species were responsible for the oxidative coupling of methane via a redox mechanism [6,7] and molecular oxygen is activated by an F center to produce lattice oxygen [8]. It was suggested that the surface of the catalyst was dominated by oxygen-enriched amorphous phases consisting of discretely distributed tetrahedral WO_4 and octahedral MnO_6 groups [12]. There is evidence for a synergic effect among the sodium, tungsten, and manganese components. The active oxygen species of the catalyst was proposed to be mobile surface lattice oxygen supplied by tungsten and manganese oxides, and it was suggested that the sodium strongly polarizes the metal–oxygen bonds of the tungsten and manganese oxides, increasing the mobility of the surface lattice oxygen [15–21]. In a 200-ml fluidized bed reactor under the reaction conditions of 800–875 °C, CH_4:O_2:H_2O = 6:1:3, and GHSV(CH_4) = 7000 h^{-1}, the catalyst was successfully tested for 450 h, giving a C_2 yield of 17.8–19.4% and a C_2 selectivity at 75.7–82.6% [9,10]. At elevated pressure, the catalyst exhibited not only the same catalytic activity and C_2 selectivity, but also a higher ratio of C_2H_4 to C_2H_6 when the space velocity was increased [11]. More recently, the CeO_2- and SnO_2-promoted Na–W–Mn/SiO_2 catalysts for the oxidative conversion of methane have been studied

* Corresponding author.
E-mail address: malcolm.green@chem.ox.ac.uk (M.L.H. Green).
[1] Current address: Johnson Matthey Technology Centre, Blount's Court, Sonning Common, Reading, RG4 9NH, UK.

0021-9517/$ – see front matter
doi:10.1016/S0021-9517(03)00248-3

in a micro-stainless-steel reactor under elevated pressure [22–24]. A CH_4 conversion of 47.2% with a C_2–C_4 selectivity of 47.3% (C_2:C_3:C_4 = 1:1:3.3) was obtained at 710 °C with 1.0×10^5 ml g^{-1} h^{-1} GHSV, $CH_4/O_2 = 2.5$, and $P = 0.6$ MPa. In addition, the Na_2WO_4–Mn/SiO_2 catalysts also exhibited a good activity for the conversion of CH_4 with CO_2 into C_2 hydrocarbon [13] and for the oxidative dehydrogenation of ethane using oxygen and carbon dioxide as oxidants [14].

The same catalyst system has been studied by Lunsford [25–30], Lambert [31,32], and Abedini [33]. Lunsford and co-workers suggested that a Na–O–Mn species was mainly responsible for the activation of methane, and that sodium was responsible for preventing the complete oxidation of CH_4. The presence of tungstate ions appears to impart stability to the catalyst [25,26]. In a recycle mode with continuous removal of alkenes, yields of ethylene over 70% have been achieved [27,28] using a Na_2WO_4–Mn/SiO_2 catalyst. Lambert and co-workers emphasized the effect of the phase transition from amorphous silica to α-cristobalite and the effect of different alkali additives on the catalytic performance, and they proposed that Na plays a dual role as both a structural and a chemical promoter. The phase transition from amorphous silica to α-cristobalite appears to be a critically important requirement for the production of an effective catalyst and incorporation of W switches on OCM activity. An alkali-stabilized tungsten oxo species is thought to be the OCM active site [31,32]. Recently, the electrical conductivity and the catalytic performance of $M/Na_2WO_4/SiO_2$ (M = V, Cr, Mn, Fe, Co, and Zn) catalysts for OCM have been studied by Abedini and co-workers [33]. The authors found the best catalytic performance for the Na_2WO_4–Mn/SiO_2 OCM catalyst system and associated this with its highest electrical conductivity due to the lowest band gap between manganese oxide and Na_2WO_4/SiO_2.

In this work, the M–W–Mn/SiO_2 catalysts (M = Li, Na, K, Ba, Ca, Fe, Co, Ni, and Al) have been prepared with the same molar content as a 5 wt% Na_2WO_4–2 wt% Mn/SiO_2 catalyst and their catalytic performances for OCM were evaluated using a continuous-flow fixed-bed reactor. The effect of different additives on the state of tungsten oxide and roles of the WO_4 tetrahedra and the WO_6 octahedra on the catalyst surface have been investigated using X-ray photoelectron spectroscopy (XPS), laser Raman spectroscopy (LRS), X-ray diffraction (XRD), and FTIR spectroscopy. Models for the interaction of the tetrahedral WO_4 and octahedral WO_6 with methane were proposed to correlate the performance of the catalyst with the additives.

2. Experimental

2.1. Catalyst preparation

The catalysts were prepared by the incipient wetness impregnation method. The silica gel support (32–53 mesh) was first impregnated with an aqueous solution of $Mn(NO_3)_2$ at 90 °C, and for 4–5 h at 120 °C, and then with aqueous solutions containing an appropriate amount of $(NH_4)_5H_7(WO_4)_6$ and $M(NO_3)$ (M = Li, Na, K, Ba, Ca, Fe, Co, Ni, and Al) at 90 °C, and then dried for 4–5 h at 120 °C. Finally, the catalysts were calcined in air for 6 h at 830–850 °C. Herein, the amounts of the various components are expressed in same molar weight as 5 wt% Na_2WO_4–2 wt% Mn/SiO_2 catalyst. The catalysts were tested for 5 h and then unloaded. During the unloading, the reactor was allowed to cool to room temperature under a flowing Ar atmosphere and then exposed to air before collection.

2.2. Catalytic activity test

Activity testing was carried out in a quartz fixed-bed microreactor (i.d. 6 mm). About 0.2 g catalyst was loaded in the reactor, and the remaining volume was filled with quartz chips so as to reduce the contribution from gas-phase reactions. A thermocouple was attached to the outside wall of the reactor to monitor the reactor temperature and to control the furnace. The reactants, CH_4 and O_2 (99.9% purity), were used without further purification. Gas flow rates were regulated with mass flow controllers (D07-11/ZM made by Beijing Sevenstar Huachuang Electronic Co. Ltd). The catalysts were evaluated at 800 °C, and 1 bar with a GHSV of 25,400 ml g^{-1} h^{-1}. The reactant consists of methane and oxygen at a ratio of 3.2:1, without any further dilution with an inert gas. These experimental conditions were applied to all activity tests. At the reactor outlet a cold trap was used to remove the water from the exit gas stream. The reaction products were then analyzed with an on-line SC-6 GC equipped with a TCD, using a Porapak Q column for the separation of CH_4, CO_2, C_2H_4, and C_2H_6, and a 5 Å molecular sieve column for the separation of O_2, CH_4, and CO.

2.3. Catalyst characterization

The XPS analysis of the catalysts was performed with a VG ESCALAB 210 spectrometer. The fresh catalyst was pressed into a self-supported wafer and treated with flowing O_2 at 800 °C for 30 min in the pretreatment chamber before it was passed into the high-vacuum analysis chamber. In the analysis of the postreaction catalyst, samples were degassed at room temperature in the pretreatment chamber without heating in an O_2 atmosphere. A Mg target was used as the anode of the X-ray source with a power of 300 W. The pass energy of the analyzer was 25 eV in a step increment of 0.05 eV. The binding energies were calibrated using the Si (2p) line at 103.4 eV as the reference. Near-surface compositions were calculated from peak areas using sensitivity factors, which were provided in the software of the instrument.

The Raman spectra of the catalysts were recorded in a Yuon Jobin Labram 300 spectrometer with a resolution of

2 cm^{-1}. It is equipped with a CCD camera enabling microanalysis on a sample point. A 514.5 nm Ar^+ laser source was used and the spectra were acquired in a back-scattered confocal arrangement. The scanning range was set from 90 to 3000 cm^{-1}.

The XRD patterns of the catalysts were obtained with a Philips PW1710 diffractometer using Cu-K_α radiation X-ray at 40 eV and 30 mA. All samples were mounted on an aluminum plate with a groove cut into it and measured at room temperature.

The IR spectra of the catalysts were recorded in a Bruker IFS 120HR FTIR spectrometer with a resolution of 2 cm^{-1} and 64 scans for each spectrum. It is equipped with a MCT detector. The scanning range was set from 4000 to 400 cm^{-1}.

3. Results

3.1. Catalytic reaction results

The results of CH_4 conversion and product selectivity of the M–W–Mn/SiO_2 catalysts (M = Li, Na, K, Ba, Ca, Fe, Co, Ni, and Al) for OCM are listed in Table 1. Over the Na– and K–W–Mn/SiO_2 catalysts, CH_4 conversion and C_2H_4 selectivity are approximately 30 and 40%, respectively. After 5 h time on stream, the performance of the catalysts was essentially unchanged. With the Li–W–Mn/SiO_2 catalyst, the CH_4 conversion was only 20%, and the C_2H_4 selectivity 35.4%. After 5 h time on stream, there was a small decrease for CH_4 conversion, but the C_2H_4 selectivity is decreased dramatically and C_2H_6 selectivity is decreased slightly. For the Ba–W–Mn/SiO_2 catalyst, the CH_4 conversion and C_2H_4 selectivity were 21.3 and 18.7% after a 0.5 h test; however, CO selectivity was up to 45.5%. After testing for 5 h, CH_4 conversion and C_2H_6 selectivity decreased to 18.6 and 13.2%. However, CO selectivity is increased. These results are in agreement with the literature [30–36]: the presence of Na and K additives helps to maintain the catalyst activity and selectivity while the addition of Li and Ba did not improve the catalyst activity, selectivity, and stability.

Over the Ca–, Fe–, Co–, Ni–, and Al–W–Mn/SiO_2 catalysts, both CH_4 conversion and C_2 selectivity were low, with a high selectivity to CO. After an activity test of 5 h, the CH_4 conversion and product selectivities did not change significantly. These results showed that the addition of the transition metal did not improve the catalyst performance for the methane oxidative coupling to ethylene.

Sofranko and co-workers [34–36] have reported that the performance of manganese oxide/silica OCM catalysts (without tungsten) can be improved by the addition of alkali metals and alkaline earths. They obtained the highest C_2 selectivity with sodium as a promoter and believed that the effect of Na^+ ions was to increase surface basicity and convert nonselective manganese oxide into a more selective form. The results in Table 1 show that the effect of alkali metals ions is stronger than that of the alkaline earth ions and the other metal ions for OCM catalysts.

The surface areas of the M–W–Mn/SiO_2 are given in Table 2. Interestingly, there is no significant difference between the fresh and the postreaction catalysts, indicating that the reaction does not change the surface area of the catalysts. However, comparison of the surface areas of the Li, Na, K, Ba, and Ca-promoted W–Mn/SiO_2 catalysts and the

Table 1
The catalytic performance of the M–W–Mn/SiO_2 catalysts[a]

Catalysts[b]	Conversion of CH_4 (%)	Selectivity (%)				Yield (%)	
		C_2H_4	C_2H_6	CO	CO_2	C_{2+}	CO_x
Li_2WO_4–Mn/SiO_2	20.5	35.4	28.7	17.8	18.1	13.1	7.4
Li_2WO_4–Mn/SiO_2[c]	18.2	25.7	27.6	25.2	21.5	9.7	8.5
Na_2WO_4–Mn/SiO_2	29.5	42.6	23.8	11.5	22.1	19.6	9.9
Na_2WO_4–Mn/SiO_2[c]	28.9	43.9	22.7	11.6	21.8	19.3	9.6
K_2WO_4–Mn/SiO_2	29.6	39.6	22.8	12.7	24.9	18.5	11.1
K_2WO_4–Mn/SiO_2[c]	29.8	39.7	22.7	13.3	24.3	18.6	11.2
$BaWO_4$–Mn/SiO_2	21.3	18.7	13.8	45.5	22.0	6.9	14.4
$BaWO_4$–Mn/SiO_2[c]	18.6	13.2	12.5	51.0	23.3	4.8	13.8
$CaWO_4$–Mn/SiO_2	19.0	12.1	13.2	55.2	19.5	4.8	14.2
$CaWO_4$–Mn/SiO_2[c]	18.2	11.4	13.6	54.3	20.7	4.6	13.6
$FeWO_4$–Mn/SiO_2	18.3	7.5	7.1	67.3	18.1	2.7	15.6
$FeWO_4$–Mn/SiO_2[c]	17.7	7.5	7.6	67.1	17.8	2.7	15.0
$CoWO_4$–Mn/SiO_2	18.3	11.9	11.1	56.1	20.9	4.2	14.1
$CoWO_4$–Mn/SiO_2[c]	18.1	11.1	12.7	56.4	19.8	4.3	13.8
$NiWO_4$–Mn/SiO_2	18.4	12.1	11.7	52.3	23.9	4.4	14.0
$NiWO_4$–Mn/SiO_2[c]	17.9	10.6	9.9	56.7	22.8	3.7	14.2
$Al_2(WO_4)_3$–Mn/SiO_2	17.9	8.6	8.0	68.1	15.3	3.0	14.9
$Al_2(WO_4)_3$–Mn/SiO_2[c]	17.1	8.4	8.3	69.3	14.0	2.9	14.2

[a] Reaction conditions: $T = 800\,^\circ C$; CH_4:O_2 = 3.2:1; GHSV = 25,400 ml g^{-1} h^{-1}; 0.2 g catalyst; stream time = 0.5 h.
[b] The molecular formula of the metal tungstate was identified by XRD.
[c] Reaction conditions: $T = 800\,^\circ C$; CH_4:O_2 = 3.2:1; GHSV = 25,400 ml g^{-1} h^{-1}; 0.2 g catalyst; stream time = 5 h.

Table 2
Observed XPS binding energies (eV) and near-surface compositions (at.%) of the M–W–Mn/SiO_2 catalyst components

Catalysts	M[a]		W(4f)		Mn(2p)		Si(2p)		O(1s)(SiO_2)		O(1s)(MO_x)[b]		Surface area
	BE (eV)	at.%	BE (eV)	at.%	BE (eV)	at.%	BE (eV)	at.%	BE (eV)	at.%	BE (eV)	at.%	M^2/g
Li_2WO_4–Mn/SiO_2[c]	55.7	5.7	35.9	2.2	641.7	1.5	103.4	20.9	532.8	51.1	530.9	18.6	11.1
Li_2WO_4–Mn/SiO_2[d]	55.9	5.2	35.6	2.0	641.6	1.8	103.4	20.8	532.7	52.5	530.6	17.7	12.0
Na_2WO_4–Mn/SiO_2[c]	1072.2	12.8	35.7	1.6	641.5	2.3	103.4	19.9	532.9	49.7	530.8	13.7	28.7
Na_2WO_4–Mn/SiO_2[d]	1072.1	12.6	35.8	1.5	641.4	2.4	103.4	19.2	532.9	49.5	530.9	14.8	27.6
K_2WO_4–Mn/SiO_2[c]	293.3	7.1	35.6	1.5	641.7	1.4	103.4	21.1	532.8	51.0	531.0	17.9	43.8
K_2WO_4–Mn/SiO_2[d]	293.4	7.5	35.7	1.6	641.5	1.7	103.4	21.5	532.9	50.2	530.9	17.5	42.9
$BaWO_4$–Mn/SiO_2[c]	780.1	4.8	35.7	2.2	641.5	1.1	103.4	20.0	532.9	49.8	530.9	22.1	244.12
$BaWO_4$–Mn/SiO_2[d]	779.9	4.3	35.3	2.3	641.3	1.5	103.4	20.1	532.8	50.3	530.5	21.5	241.35
$CaWO_4$–Mn/SiO_2[c]	347.5	0.5	35.1	1.1	641.8	1.2	103.4	24.7	532.7	56.8	531.6	15.7	231.79
$CaWO_4$–Mn/SiO_2[d]	347.3	0.7	35.1	1.2	641.7	1.3	103.4	24.9	532.9	56.5	531.4	15.4	235.65
$FeWO_4$–Mn/SiO_2[c]	710.4	0.4	35.2	1.1	641.6	1.1	103.4	25.1	532.8	50.6	531.5	21.7	272.87
$FeWO_4$–Mn/SiO_2[d]	710.3	0.5	35.1	1.2	641.6	1.5	103.4	25.2	532.8	50.1	531.5	21.5	269.30
$CoWO_4$–Mn/SiO_2[c]	781.3	1.5	35.0	1.7	641.2	1.5	103.4	20.7	532.9	55.8	530.4	18.8	243.39
$CoWO_4$–Mn/SiO_2[d]	781.5	1.4	35.0	1.7	641.3	1.8	103.4	20.5	532.8	55.6	530.5	19.0	245.80
$NiWO_4$–Mn/SiO_2[c]	855.8	0.8	35.0	2.0	640.9	2.1	103.4	19.7	532.8	55.5	530.2	19.9	246.94
$NiWO_4$–Mn/SiO_2[d]	855.6	0.9	35.0	2.1	640.8	2.3	103.4	19.3	532.7	55.3	530.2	20.1	239.75
$Al_2(WO_4)_3$–Mn/SiO_2[c]	73.9	1.2	35.0	1.8	640.8	1.8	103.4	21.5	532.8	59.8	530.2	13.9	249.19
$Al_2(WO_4)_3$–Mn/SiO_2[d]	74.0	1.1	35.1	1.8	640.8	1.9	103.4	21.0	532.8	59.5	530.1	14.7	242.32

[a] Li_2WO_4–Mn/SiO_2, Na_2WO_4–Mn/SiO_2, K_2WO_4–Mn/SiO_2, $BaWO_4$–Mn/SiO_2, $CaWO_4$–Mn/SiO_2, $FeWO_4$–Mn/SiO_2, $CoWO_4$–Mn/SiO_2, $NiWO_4$–Mn/SiO_2, and $Al_2(WO_4)_3$–Mn/SiO_2 catalysts are Li(1s), Na(1s), K(2p), Ba(3d), Ca(2p), Fe(2p), Co(2p), Ni(2p), and Al(2p), respectively.
[b] MO_x represents the metal oxides except SiO_2.
[c] Fresh catalysts.
[d] After testing 5 h ($T = 800\,^\circ$C; CH_4:O_2 = 3.2:1; GHSV = 25,400 ml g^{-1} h^{-1}; 0.2 g catalyst).

Fe-, Co-, Ni-, and Al-modified catalysts suggests that the alkali and alkaline earth metal-promoted catalysts have a much smaller surface area than those of the aluminum and transition metal-modified catalysts. This can be explained by the promotion effect on the transition of amorphous silica into α-cristobalite by the addition of the alkali or alkaline earth metal or the formation of silicate compounds. Crystalline α-cristobalite abd silicate compounds are low surface area materials.

3.2. X-ray photoelectron spectroscopy

Table 2 shows the observed binding energies and near-surface elemental compositions of the fresh and the postreaction catalysts. In the fresh catalysts, the near-surface concentration of Mn is between 1.1 and 2.3%, and this does not correlate directly with the observed CH_4 conversions and product selectivities. After the catalyst was tested for 5 h, the near-surface concentrations of Mn in all of the catalysts are higher than in the fresh catalysts, suggesting that some Mn surface migration occurs during the OCM reaction. In the fresh catalysts, the near-surface concentration of W is between 1.1 and 2.2%, and those of the metal ions is between 0.4 and 12.8%, significantly varying with different catalysts. The near-surface concentrations of Li, Na, K, and Ba are relatively higher than the stoichiometric composition of metal tungstate, while those of Ca, Fe, Co, Al, and Ni are lower than the stoichiometric tungstate composition. These results indicate that the Li, Na, K, and Ba are enriched, and Ca, Fe, Co, Al, and Ni are deficient in the catalyst surface.

The binding energy of W(4f) also changes with the different additives. Generally speaking, the alkali and alkaline-earth metal-modified catalysts have the higher W(4f) binding energy: the W(4f) binding energy over the fresh and used Na–W–Mn/SiO_2 was 35.8 eV, while the Ca-modified catalyst has the lowest W(4f) binding energy among the alkali and alkaline-earth metal-modified catalysts, only 35.2 eV. In comparison to the alkali and alkaline-earth metal-modified catalysts, the transition metal-modified W–Mn/SiO_2 catalysts have lower W(4f) binding energy, less than 35.2 eV.

3.3. Laser Raman spectroscopy

The Raman spectra of the fresh and the postreaction catalysts are shown in Fig. 1. The laser Raman spectrum of unpromoted 3.1% W–2% Mn/SiO_2 was measured and listed as a reference to compare the addition of the different metal modifiers on the vibration of the catalyst surface. Comparison with the literature results [18,37–39] suggests that the Raman bands between 952 and 905 cm^{-1} can be assigned to tetrahedral WO_4, and bands between 889 and 862 cm^{-1} to octahedral WO_6. The bands at 701 and 574 cm^{-1} are attributed to manganese oxide species, and those below 500 cm^{-1} to α-cristobalite and quartz (Ref. [18] and Fig. 1A, a).

It can be seen from Fig. 1 that the fresh Na–W–Mn/SiO_2 catalyst has two bands at 947 and 905 cm^{-1} due to the tetrahedral WO_4, and there are four bands at 683, 615, 574, and 509 cm^{-1} due to manganese oxide species, while no Raman bands assignable to octahedral WO_6 were observed

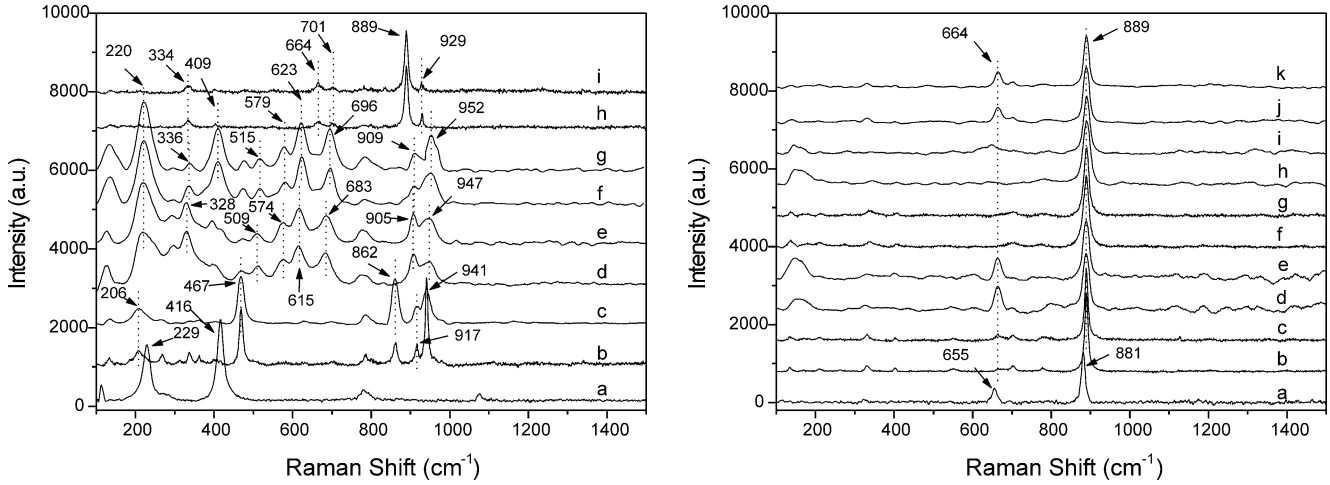

Fig. 1. (A) The Raman spectra of (a) α-cristobalite, (b) Li–W–Mn/SiO_2 (fresh), (c) Li–W–Mn/SiO_2 (post), (d) Na–W–Mn/SiO_2 (fresh), (e) Na–W–Mn/SiO_2 (post), (f) K–W–Mn/SiO_2 (fresh), (g) K–W–Mn/SiO_2 (post), (h) Ba–W–Mn/SiO_2 (fresh), and (i) Ba–W–Mn/SiO_2 (post) catalysts. (B) The Raman spectra of (a) 3.1% W–2% Mn/SiO_2, (b) Ca–W–Mn/SiO_2 (fresh), (c) Ca–W–Mn/SiO_2 (post), (d) Fe–W–Mn/SiO_2 (fresh), (e) Fe–W–Mn/SiO_2 (post), (f) Co–W–Mn/SiO_2 (fresh), (g) Co–W–Mn/SiO_2 (post), (h) Ni–W–Mn/SiO_2 (fresh), (i) Ni–W–Mn/SiO_2 (post), (j) Al–W–Mn/SiO_2 (fresh), and (k) Al–W–Mn/SiO_2 (post) catalysts.

(Fig. 1A, d). The fresh K–W–Mn/SiO_2 catalyst has two bands at 952 and 909 cm^{-1} (for tetrahedral WO_4), and four bands at 696, 623, 579, and 515 cm^{-1} (for manganese oxide species). Again no Raman bands for octahedral WO_6 were observed (Fig. 1A, f). After an activity test for 5 h, no change was observed in the Raman bands assigned to the tetrahedral WO_4 and manganese oxide species, suggesting that the surface structure of the catalysts is not changed during the 5 h test.

The fresh Li–W–Mn/SiO_2 catalyst has two bands at 941 and 917 cm^{-1} due to tetrahedral WO_4, one at 862 cm^{-1} for octahedral WO_6, and one strong band at 467 cm^{-1} and one weak band at 206 cm^{-1} for quartz SiO_2; no Raman bands due to the manganese oxide species could be seen (Fig. 1A, b). After an activity test for 5 h, the band at 941 cm^{-1} for the tetrahedral WO_4 decreased greatly while the band at 862 cm^{-1} (octahedral WO_6) increased significantly (Fig. 1A, c), indicating that the surface structure of the catalyst had changed under the OCM reaction conditions. Comparison with the catalytic activity of the Li–W–Mn/SiO_2 catalyst (entries 1 and 2, Table 1) shows that the fresh catalyst has a good initial CH_4 conversion activity and C_2 selectivity but, after a 5-h test, the CH_4 conversion and C_2H_4 selectivity decreased greatly, suggesting that the WO_4 tetrahedron on the catalyst surface may play an important role in the CH_4 conversion and the C_2H_4 selectivity.

The fresh Ba–W–Mn/SiO_2 catalyst has one weak band at 929 cm^{-1} for the tetrahedral WO_4, one strong band at 889 cm^{-1} for the octahedral WO_6, and two weak bands at 701 and 664 cm^{-1} for the manganese oxide (Fig. 1A, h). This catalyst exhibited a quite high activity for CH_4 conversion and C_2H_4 selectivity (entries 7 and 8, Table 1). After an activity test of 5 h, the Raman band at 929 cm^{-1} for tetrahedral WO_4 decreased (Fig. 1A, i) and the CH_4 conversion decreased slightly, while the C_2H_4 selectivity dropped rapidly. This further suggests that the tetrahedral WO_4 plays a key role for the CH_4 conversion and C_2H_4 selectivity.

The Ca–, Fe–, Co–, Ni–, and Al–W–Mn/SiO_2 catalysts each had a band at 890 cm^{-1} for octahedral WO_6, no Raman bands due to the tetrahedral WO_4, and only a weak peak at 664 cm^{-1} for the manganese oxide system in some catalysts (Fig. 1B, b, d, f, h, and j). However, the 3.1% W–2% Mn/SiO_2 catalyst has one peak at 881 cm^{-1} for octahedral WO_6 and a weak band at 655 cm^{-1} for manganese oxide species (Ref. [18] and Fig. 1B, a). It can be seen that in the WO_6 octahedra-containing catalysts, formulated using Ca, Fe, Co, Ni, and Al, the CH_4 conversion was less than in the Na and K-promoted catalysts, and the C_2 selectivity was poor while the CO selectivity was very high. After an activity test for 5 h, the activity of the catalysts is almost the same and the Raman spectra are not changed significantly (Fig. 1B, c, e, g, i, and k), suggesting that the surface structure of these catalysts is stable under the reaction conditions.

In summary, comparison of the catalytic performance with Raman bands of all fresh and postreaction catalysts reveals a correlation between the presence of tetrahedral WO_4 and the high CH_4 conversion and C_2 selectivity; therefore, tetrahedral WO_4 species appear to be an essential ingredient in the formulation of an efficient OCM catalyst based on the M–W–Mn/SiO_2 catalyst system. Furthermore, tetrahedral WO_4 appear to be stabilized in the Na– and K–W–Mn/SiO_2 catalysts, which has α-cristobalite support. However, the tetrahedral WO_4 is unstable in Li– or Ba–W–Mn/SiO_2 catalyst, which has a quartz SiO_2 or amorphous SiO_2 as the support, even though the alkali metal ion or alkaline earth metal ion, tungsten, and manganese coexist in the catalysts.

Table 3
Phase identification and crystal size of the M–W–Mn/SiO_2 catalysts

Catalysts[a]	Crystal phases	Size (μm)	Crystal phases	Size (μm)
Li_2WO_4–Mn/SiO_2[b]	Li_2WO_4	2.03	Mn_2O_3	1.39
Li_2WO_4–Mn/SiO_2[c]	Li_2WO_4	2.16	Mn_2O_3	1.46
Na_2WO_4–Mn/SiO_2[b]	Na_2WO_4	0.51	Mn_2O_3	0.87
Na_2WO_4–Mn/SiO_2[c]	Na_2WO_4	0.49	Mn_2O_3	0.89
K_2WO_4–Mn/SiO_2[b]	K_2WO_4	2.89	Mn_2O_3	0.58
K_2WO_4–Mn/SiO_2[c]	K_2WO_4	2.90	Mn_2O_3	0.61
$BaWO_4$–Mn/SiO_2[b]	$BaWO_4$	0.38	$MnWO_4$	0.34
$BaWO_4$–Mn/SiO_2[c]	$BaWO_4$	0.32	$MnWO_4$	0.39
$CaWO_4$–Mn/SiO_2[b]	$CaWO_4$	0.60	$MnWO_4$	0.48
$CaWO_4$–Mn/SiO_2[c]	$CaWO_4$	0.63	$MnWO_4$	0.51
$FeWO_4$–Mn/SiO_2[b]	$FeWO_4$	1.05	$MnWO_4$	0.62
$FeWO_4$–Mn/SiO_2[c]	$FeWO_4$	1.09	$MnWO_4$	0.71
$CoWO_4$–Mn/SiO_2[b]	$CoWO_4$	0.39	$MnWO_4$	0.39
$CoWO_4$–Mn/SiO_2[c]	$CoWO_4$	0.41	$MnWO_4$	0.37
$NiWO_4$–Mn/SiO_2[b]	$NiWO_4$	0.35	$MnWO_4$	0.67
$NiWO_4$–Mn/SiO_2[c]	$NiWO_4$	0.33	$MnWO_4$	0.72
$Al_2(WO_4)_3$–Mn/SiO_2[b]	$Al_2(WO_4)_3$	0.52	$MnWO_4$	0.48
$Al_2(WO_4)_3$–Mn/SiO_2[c]	$Al_2(WO_4)_3$	0.49	$MnWO_4$	0.56

[a] The crystalline phases were identified by XRD according to the Scherrer equation: $D = K\lambda/B_{1/2}\cos\theta$.

[b] Before reaction.

[c] After reaction (reaction conditions: $T = 800\,^{\circ}\mathrm{C}$; $CH_4{:}O_2 = 3.2{:}1$; GHSV = 25,400 ml g^{-1} h^{-1}; 0.2 g catalyst; stream time = 5 h).

3.4. X-ray diffraction

The phase composition and crystal size of the different catalysts before and after reaction are summarized in Table 3. It can be seen that in the alkali metal-modified catalysts, the main crystalline phases are M_2WO_4 and Mn_2O_3, and these do not change significantly after the activity test for 5 h. Although the surface areas of the supports are very similar, there is a significant difference among the particle sizes of the crystalline phases. Comparison with the catalyst performance shows that the crystal size of the M_2WO_4 and MO_3 does not exert a significant effect on the catalyst performance.

While in the alkaline–earth and transition metal-modified catalysts, the main crystalline phases of the catalyst are M_2WO_4 and Mn_2O_3. The crystallite size does not change after the reaction test, but the size of the crystallite differs with the catalysts. Although the crystallite sizes of Na_2WO_4 and K_2WO_4 are 0.51 and 2.89 nm, they have a similar performance for methane conversion and C_2H_4 selectivity. Hence it is inferred that the crystallite size is not directly related to catalyst performance.

The XRD patterns of the fresh and the postreaction catalysts are shown in Fig. 2. In the fresh Na–W–Mn/SiO_2 catalyst, Na_2WO_4, $Na_2W_2O_7$, Mn_2O_3, and α-cristobalite phases are detected. In the fresh K–W–Mn/SiO_2 catalyst, K_2WO_4, Mn_2O_3, and α-cristobalite phases are present. After OCM activity testing for 5 h, these phases are still present in the catalysts. In the fresh Li–W–Mn/SiO_2 catalyst, Li_2WO_4, Li_6WO_6, Mn_2O_3, and quartz SiO_2 phases are detected. In the catalyst tested for 5 h the Li_2WO_4 phase decreased while the Li_6WO_6 phase slightly increased, indicating that the Li_2WO_4 phase is unstable under the OCM reaction conditions.

XRD results show that the fresh Ba–W–Mn/SiO_2 catalyst is composed of $BaWO_4$, $MnWO_4$, and amorphous SiO_2 phases. No Mn_2O_3 phase was detected. This indicates that in this catalyst, Mn has been converted into the $MnWO_4$ phase.

Literature results [37] show that tungsten is tetrahedral WO_4 in $BaWO_4$, and octahedral WO_6 in $MnWO_4$. In the fresh Ba–W–Mn/SiO_2 catalyst, the amount of the $BaWO_4$ phase was greater than the $MnWO_4$ phase. Our laser Raman results suggest that the tetrahedral WO_4 species is less abundant than the octahedral WO_6. These results indicate that $BaWO_4$ is mainly present in the subsurface of the catalyst and $MnWO_4$ is distributed on the catalyst surface. After activity testing for 5 h, the $BaWO_4$ phase decreased in content and the $MnWO_4$ phase increased slightly, suggesting that the $BaWO_4$ phase is unstable under OCM reaction conditions.

In the Ca–, Fe–, Co–, Ni–, and Al–W–Mn/SiO_2 catalysts, more $MnWO_4$ phase and less metal tungstate phase was detected and, after activity testing for 5 h, the abundance of these phases did not change significantly. The catalyst systems are stable and experience little change during the activity tests.

3.5. FTIR spectroscopy

Although the IR bands of the metal tungstate and manganese oxide species in the catalysts cannot be separated, the IR bands of α-cristobalite, amorphous SiO_2, and quartz SiO_2 are distinguishable. Therefore, information regarding the interaction of tetrahedral WO_4 and octahedral WO_6 with the support in the catalysts can be inferred from changes in

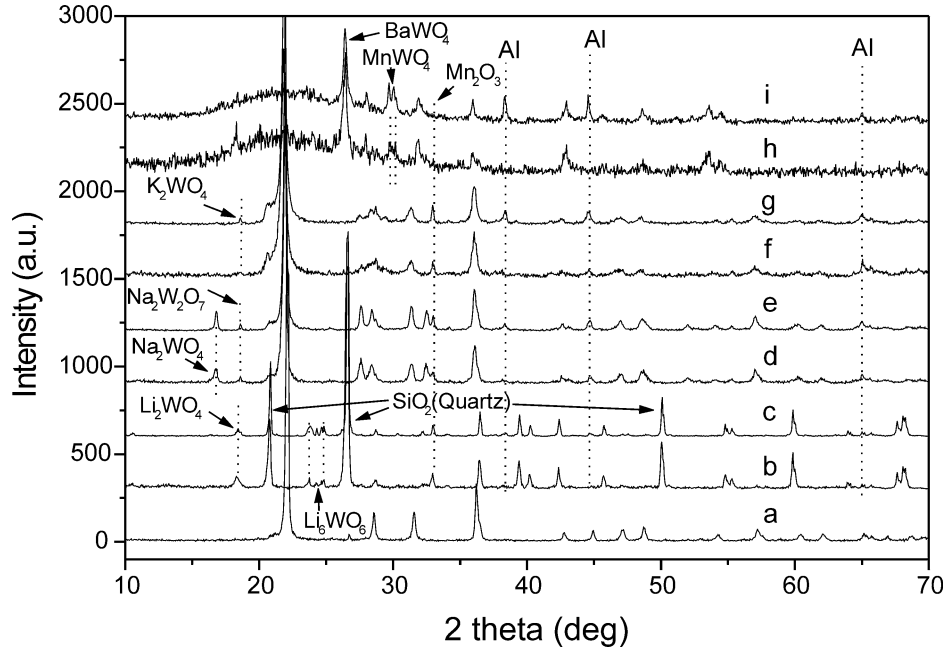

(A)

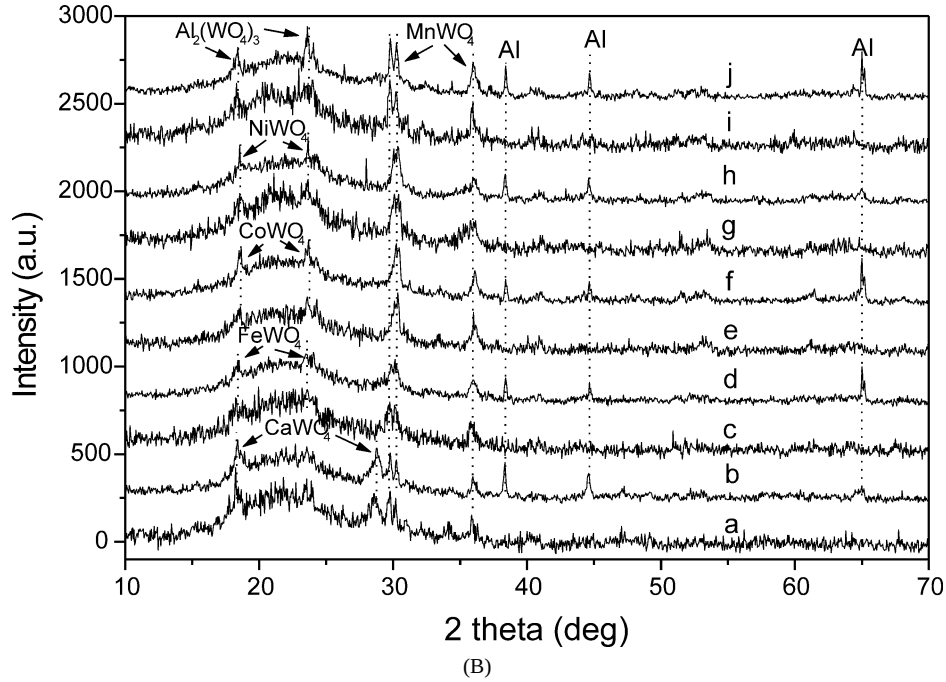

(B)

Fig. 2. (A) The XRD pattern of (a) α-cristobalite, (b) Li–W–Mn/SiO_2 (fresh), (c) Li–W–Mn/SiO_2 (post), (d) Na–W–Mn/SiO_2 (fresh), (e) Na–W–Mn/SiO_2 (post), (f) K–W–Mn/SiO_2 (fresh), (g) K–W–Mn/SiO_2 (post), (h) Ba–W–Mn/SiO_2 (fresh), and (i) Ba–W–Mn/SiO_2 (post) catalysts. (Al refers to the peaks from the aluminum sample holder.) (B) The XRD pattern of (a) Ca–W–Mn/SiO_2 (fresh), (b) Ca–W–Mn/SiO_2 (post), (c) Fe–W–Mn/SiO_2 (fresh), (d) Fe–W–Mn/SiO_2 (post), (e) Co–W–Mn/SiO_2 (fresh), (f) Co–W–Mn/SiO_2 (post), (g) Ni–W–Mn/SiO_2 (fresh), (h) Ni–W–Mn/SiO_2 (post), (i) Al–W–Mn/SiO_2 (fresh), and (j) Al–W–Mn/SiO_2 (post) catalysts. (Al refers to the peaks from the aluminum sample holder.)

the IR spectra of SiO_2. The IR spectra of the fresh and the postreaction catalysts are shown in Fig. 3. The IR bands of the α-cristobalite are at 1200, 1092, 793, 619, and 483 cm^{-1} (Fig. 3A, a). In the fresh Na–W–Mn/SiO_2 catalyst, bands are present at 1198, 1099, 795, 619, and 494 cm^{-1} (Fig. 3A, d), and in the fresh K–W–Mn/SiO_2 catalyst, they are at 1198, 1099, 795, 619, and 487 cm^{-1} (Fig. 3A, f). Comparing the IR bands of the catalysts with the α-cristobalite reveals that the presence of tetrahedral WO_4 brings about a change in the IR bands of the α-cristobalite, except the IR band at 619 cm^{-1}. This indicates a close interaction of the tetrahedral WO_4 with α-cristobalite. After activity testing for 5 h, the IR bands of the catalysts are not changed, demonstrating that the tetrahedral WO_4 are stable with α-cristobalite.

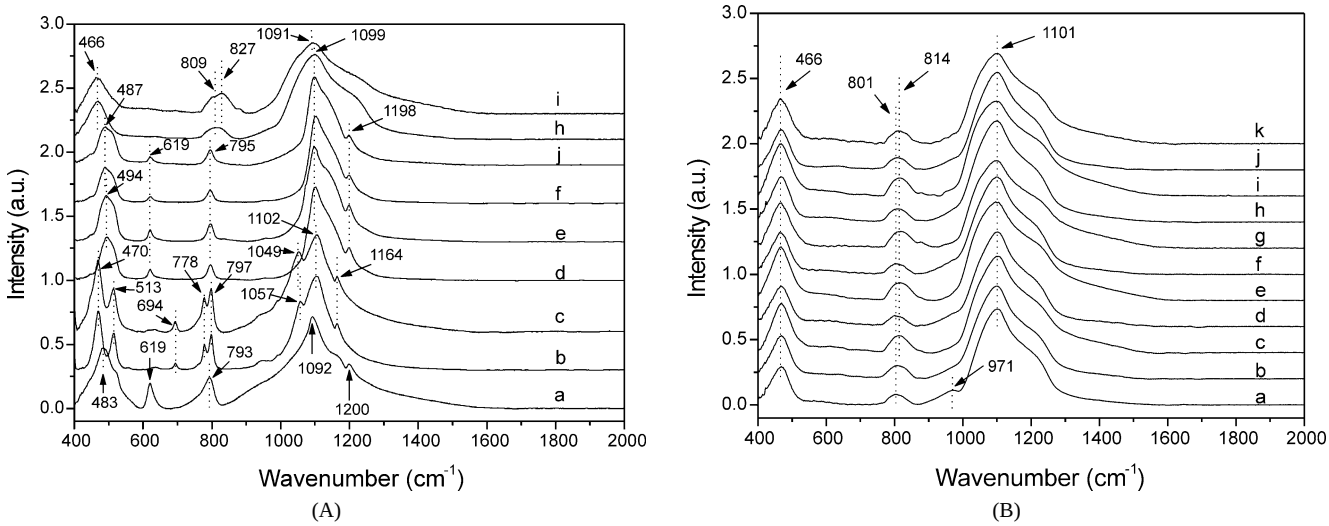

Fig. 3. (A) The FTIR spectra of (a) α-cristobalite, (b) Li–W–Mn/SiO_2 (fresh), (c) Li–W–Mn/SiO_2 (post), (d) Na–W–Mn/SiO_2 (fresh), (e) Na–W–Mn/SiO_2 (post), (f) K–W–Mn/SiO_2 (fresh), (g) K–W–Mn/SiO_2 (post), (h) Ba–W–Mn/SiO_2 (fresh), and (i) Ba–W–Mn/SiO_2 (post) catalysts. (B) The FTIR spectra of (a) amorphous SiO_2, (b) Ca–W–Mn/SiO_2 (fresh), (c) Ca–W–Mn/SiO_2 (post), (d) Fe–W–Mn/SiO_2 (fresh), (e) Fe–W–Mn/SiO_2 (post), (f) Co–W–Mn/SiO_2 (fresh), (g) Co–W–Mn/SiO_2 (post), (h) Ni–W–Mn/SiO_2 (fresh), (i) Ni–W–Mn/SiO_2 (post), (j) Al–W–Mn/SiO_2 (fresh), and (k) Al–W–Mn/SiO_2 (post) catalysts.

The IR bands of the fresh Li–W–Mn/SiO_2 catalyst occur at 1164, 1099, 1057, 797, 778, 694, 513, and 470 cm^{-1} (Fig. 3A, b). After activity testing for 5 h, the IR band shifts from 1057 to 1049 cm^{-1} and no changes occur to the other bands. From Raman spectra (Fig. 1A, c), the tetrahedral WO_4 decreased in the Li–W–Mn/SiO_2 catalyst after a 5-h activity test, suggesting that the interaction of the tetrahedral WO_4 with the quartz SiO_2 is weak and the tetrahedral WO_4 is unstable in this system.

The IR bands of the amorphous SiO_2 are at 1101, 971, 801, and 466 cm^{-1} (Fig. 3B, a). In the fresh Ba–W–Mn/SiO_2 catalyst, they are at 1099, 809, and 466 cm^{-1} (Fig. 3A, h). It is found that the band at 971 cm^{-1} disappears and the band at 1101 shifts to a lower wavenumber (1099 cm^{-1}) and the band at 801 cm^{-1} shifts to a higher wavenumber (809 cm^{-1}). These results indicate that the interactions of the metal tungstate, manganese oxide, and the amorphous SiO_2 are strong in the catalyst. After activity testing for 5 h, the IR bands of the catalyst are at 1091, 827, and 466 cm^{-1} (Fig. 3A, i). It is found that the bands in the fresh catalyst at 1099 cm^{-1} shift to lower wavenumber (1091 cm^{-1}) and the band at 809 cm^{-1} shifts to a higher wavenumber (827 cm^{-1}), suggesting that the interactions of the metal tungstate, manganese oxide, and the amorphous SiO_2 are changed under OCM reaction conditions.

The IR bands of the fresh Ca–, Fe–, Co–, Ni–, and Al–W–Mn/SiO_2 catalysts appear at 1101, 801, and 466 cm^{-1} (Fig. 3B, b, d, f, h, and j). By comparison with the IR bands of the amorphous SiO_2 (Fig. 3B, a), it is found that the bands do not change except that at 971 cm^{-1}. Raman spectra (Fig. 1B, b, d, f, h, and j) suggests that octahedral WO_6 is present in these catalysts, revealing that the interaction of the octahedral WO_6 and the amorphous SiO_2 is weak. After activity testing for 5 h, the bands appear at 1101, 814, and 466 cm^{-1} (Fig. 3B, c, e, g, i, and k). A comparison with the fresh catalysts (Fig. 3B, b, d, f, h, and j) shows that the band at 801 cm^{-1} shifts to a higher wavenumber (814 cm^{-1}) and the other bands do not change. This means that the interaction of the octahedral WO_6 and the amorphous SiO_2 has changed and the octahedral WO_6 that exist in the amorphous SiO_2 is unstable under OCM reaction conditions.

4. Discussion

The catalytic performance of several reported OCM catalyst systems are listed in Table 4. This clearly shows the potential importance of tetrahedral WO_4 in achieving high CH_4 conversion and C_2 selectivity. In Wu's study [7], CH_4 conversion was similar over both Na^+–WO_3/SiO_2(I) (containing WO_4 tetrahedra) and Na^+–WO_3/SiO_2(II) (containing WO_6 octahedra). However, the C_2 selectivity of the catalyst containing the WO_4 tetrahedron was nearly sixfold higher than that of the catalyst containing WO_6 octahedron. In Lambert's study [31], the C_2 selectivity in the Na_2WO_4/α-cristobalite catalyst, which contains WO_4 tetrahedron, was ninefold higher than in the $(NH_4)_2WO_4$/α-cristobalite catalyst containing WO_6 octahedra. It is believed that the WO_4 tetrahedron exists in the Na_2WO_4/α-cristobalite and the WO_6 octahedron in the $(NH_4)_2WO_4$/α-cristobalite; although the structure of tungsten oxide in Na_2WO_4/α-cristobalite and $(NH_4)_2WO_4$/α-cristobalite catalysts cannot be separated using Raman spectra, some evidence has been obtained in our previous study [18]. Almost all the activity test results on this catalyst system show that the catalysts containing the WO_4 tetrahedron exhibit better performance for CH_4 conversion and C_2 selectivity than the catalysts containing the WO_6 octahedron in the metal–

Table 4
The catalytic performance of several OCM catalyst systems

Catalysts	Structure of tungsten oxide	Phase of SiO_2	Conversion of CH_4 (%)	Total C_2' selectivity (%)	C_2' yield (%)	Refs.
Na^+–WO_3/SiO_2(I)[a]	WO_4 tetrahedron	α-Cristobalite	20.6	62.9	13.0	[7]
Na^+–WO_3/SiO_2(II)[a]	WO_6 octahedron	α-Cristobalite	21.2	10.9	2.3	[7]
Na_2WO_4/α-cristobalite[b]	WO_4 tetrahedron(?)	α-Cristobalite	8	54	4.3	[31]
$(NH_4)_2WO_4/\alpha$-cristobalite[b]	WO_6 octahedron(?)	α-Cristobalite	< 5	< 5	< 0.25	[31]
0.8 wt% Na–3.1 wt% W/SiO_2[c]	WO_4 tetrahedron	α-Cristobalite	8.8	54.5	4.8	[18]
3.1 wt% W–2 wt% Mn/SiO_2[c]	WO_6 octahedron	Amorphous SiO_2	3.1	17.3	0.5	[18]
Na–, K–W–Mn/SiO_2[d]	WO_4 tetrahedron	α-Cristobalite	28.9–29.8	62.4–66.6	18.5–19.6	This work
Ca–, Fe–, Co–, Ni–, Al–W–Mn/SiO_2[d]	WO_6 octahedron	Amorphous SiO_2	17.1–19.0	14.6–25.3	2.7–4.8	This work

[a] Reaction conditions: $T = 800\,^\circ$C; CH_4:O_2 = 3:1; flow rate, 80 ml/min; weight of catalyst used, 0.2 g.
[b] Reaction conditions: $T = 850\,^\circ$C; CH_4:O_2 = 4.5:1; total flow rate = 18 ml/min; 0.4 g catalyst.
[c] Reaction conditions: $T = 800\,^\circ$C; CH_4:O_2 = 3:1; GHSV = 36,000 ml g^{-1} h^{-1}; 0.1 g catalyst.
[d] Reaction conditions: $T = 800\,^\circ$C; CH_4:O_2 = 3.2:1; GHSV = 25,400 ml g^{-1} h^{-1}; 0.2 g catalyst.

tungsten–manganese/SiO_2 catalysts. Especially, in the Li–W–Mn/SiO_2 and Ba–W–Mn/SiO_2 catalysts, the fresh catalysts containing the WO_4 tetrahedron have a good initial CH_4 conversion and C_2 selectivity. However, during the activity test for 5 h, the CH_4 conversion and C_2 selectivity dropped rapidly with a decrease in the WO_4 tetrahedron.

The reason for the apparent importance of the WO_4 tetrahedron in high CH_4 conversion and C_2 selectivity in the OCM reaction may lie in the fact that the WO_4 tetrahedron possesses suitable geometric and energy-matching properties. In the oxidative coupling of CH_4 to C_2 products under the OCM reaction conditions, it can provide active oxygen and provide a suitable site for hydrogen extraction. According to Lunsford's view [3], the first step in the oxidative coupling of methane is the removal of a hydrogen atom on the catalysts surface, leading to the creation of CH_3· radicals which can couple to form C_2 hydrocarbons. The formed CH_3· first couples to form C_2H_6, which is dehydrogenated into C_2H_4. However, the process of extracting a hydrogen atom from CH_4 proceeds with the interaction of methane with the catalyst surface, and thus forming a transition state. Hence it is inferred that the generation of the transition state is crucial for the OCM reaction.

Given that tetrahedra WO_4 and octahedra WO_6 are the active sites in the Na–W–Mn/SiO_2 catalyst for the activation of methane under the reaction conditions, they would then form the transition state in the catalytic reaction. The lowest energy principle of the system requires that CH_4 and the active sites, e.g., WO_4 or WO_6, have matching energy and geometry. The bond length of W–O in Na–W–Mn/SiO_2 is 1.77 Å [12], and C–H bond length in CH_4 is 1.106 Å [40]. In interactions between CH_4 and WO_4 or WO_6, the H atoms in CH_4 will interact with O in WO_4 and C will interact with W. Possible interaction models of WO_4 and WO_6 with methane with the low system energy are shown in Fig. 4. H_a and H_b refer to the hydrogen atoms in CH_4, which interact with different oxygen atoms in WO_4 or WO_6. These oxygen atoms are marked as O_a and O_b. The calculated structural parameters of the models are shown in Table 5.

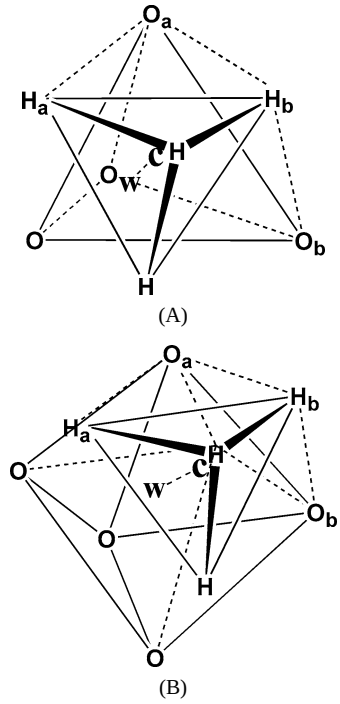

Fig. 4. (A) Scheme of the transition complex model of CH_4 with a WO_4 tetrahedron. (B) Scheme of the transition complex model of CH_4 with a WO_6 octahedron.

The calculation shows that the W–C bond length of between W in WO_4 and C in CH_4 (0.959 Å) is shorter than that between W in WO_6 and C in CH_4 (1.391 Å). Also in Fig. 4A, the bond angle of H_a–O_a–H_b (138°) is almost the same as O_a–H_b–O_b (137°), suggesting that the system is uniform and small stretching forces are present in the transition-state compounds. However, in the transition state formed by WO_6 and CH_4 (Fig. 4B), a significant difference is present between the bond angle of H_a–O_a–H_b (128°) and O_a–H_b–O_b (151°), suggesting that tension is present in the transition state. Hence it has a higher energy.

These results suggest that the transition state of WO_4 interacting with CH_4 could be more stable than that of WO_6 and methane; therefore, it is easier to present in the reac-

Table 5
The structural parameters of the transition complex of the model of the WO_4 tetrahedron and WO_6 octahedron with CH_4 tetrahedron

	Bond length of W–O[a] (Å)	Bond length of C–H[b] (Å)	Bond length of W···C (Å)	Bond angle of $H_a\cdots O_a\cdots H_b$ (deg)	Bond angle of $O_a\cdots H_b\cdots O_b$ (deg)
WO_4 tetrahedron	1.770	1.106	0.959	138	137
WO_6 octahedron	1.770	1.106	1.391	128	151

[a] From Ref. [12].
[b] From Ref. [40].

tion. Hence if more WO_4 is present in the catalyst, high activity and selectivity of the catalyst is expected. This also provides the explanation why the Na–W–Mn/SiO_2 catalysts have higher activity and selectivity than the Ca-, Fe-, Ni-, Co-, and Al-modified catalyst system.

5. Conclusions

In all the trimetallic catalysts containing alkali metal ions or alkaline-earth metal ions, tungsten, and manganese, supported on SiO_2, the presence of tetrahedral WO_4 on the catalyst surface resulted in active and selective OCM catalysts. WO_4 is present on the surface of the Na– and K–W–Mn/SiO_2 catalysts and is mainly present in the subsurface in the Ba–W–Mn/SiO_2 catalyst. It can be stabilized in the Na– and K–W–Mn/SiO_2 catalysts, which has α-cristobalite SiO_2 as the support, but is unstable in Li– or Ba–W–Mn/SiO_2 catalysts, which have quartz SiO_2 or amorphous SiO_2 as the support. FTIR spectra show that the WO_4 tetrahedron has a stronger interaction with the support than the WO_6 octahedron. A transition complex, formed by the WO_4 tetrahedron with CH_4, has been modeled, demonstrating that the WO_4 tetrahedron can have suitable geometric and energy matching with CH_4.

Acknowledgments

Support under the 973 Project of the Ministry of Science and Technology, PR China, is gratefully acknowledged (Grant G1999022406). Shengfu Ji thanks the Royal Society for a UK–China Joint Project. Tiancun Xiao thanks the Royal Society for a Royal Society BP–Amoco Fellowship.

References

[1] X. Fang, S. Li, J. Gu, D. Yang, J. Mol. Catal. (China) 6 (1992) 225.
[2] X. Fang, S. Li, J. Lin, Y. Chu, J. Mol. Catal. (China) 6 (1992) 427.
[3] J.H. Lunsford, Angew. Chem., Int. Ed. Engl. 34 (1995) 970.
[4] J.H. Lunsford, Catal. Today 63 (2000) 165.
[5] S. Li, Chin. J. Chem. 19 (2001) 16.
[6] Z. Jiang, C. Yu, X. Fang, S. Li, H. Wang, J. Phys. Chem. 97 (1993) 12870.
[7] J. Wu, S. Li, J. Phys. Chem. 99 (1995) 4566.
[8] J. Wu, S. Li, J. Niu, X. Fang, Appl. Catal. A 124 (1995) 9.
[9] J. Lin, D. Yang, J. Gu, C. Zhang, Y. Yang, Y. Chu, S. Li, J. Mol. Catal. (China) 9 (1995) 193.
[10] X. Wang, J. Zhang, D. Yang, C. Zhang, J. Lin, S. Li, Petrochem. Technol. (China) 26 (1997) 381.
[11] Y. Liu, PhD dissertation, Lanzhou Institute of Chemical Physics, Chinese Academy of Sciences, 1997.
[12] Y. Kou, B. Zhang, J. Niu, S. Li, H. Wang, T. Tanaka, S. Yoshida, J. Catal. 173 (1998) 399.
[13] Y. Liu, J. Xue, X. Liu, R. Hou, S. Li, Stud. Surf. Sci. Catal. 119 (1998) 593.
[14] Y. Liu, R. Hou, X. Liu, J. Xue, S. Li, Stud. Surf. Sci. Catal. 119 (1998) 307.
[15] S. Ji, PhD dissertation, Lanzhou Institute of Chemical Physics, Chinese Academy of Sciences, 1998.
[16] S. Ji, S. Li, C. Xu, B. Zhang, J. Mol. Catal. (China) 14 (2000) 1.
[17] S. Ji, S. Li, J. Xue, Y. Liu, C. Xu, J. Mol. Catal. (China) 14 (2000) 107.
[18] S. Ji, T. Xiao, S. Li, C. Xu, R. Hou, K.S. Coleman, M.L.H. Green, Appl. Catal. A 225 (2002) 271.
[19] S. Ji, S. Li, C. Xu, J. Xue, J. Mol. Catal. (China) 16 (2002) 204.
[20] S. Ji, S. Li, C. Xu, J. Xue, J. Mol. Catal. (China) 16 (2002) 267.
[21] S. Ji, S. Li, C. Xu, J. Xue, J. Mol. Catal. (China) 16 (2002) 310.
[22] L. Chou, Y. Cai, B. Zhang, J. Niu, S. Ji, S. Li, Chem. Commun. (2002) 996.
[23] L. Chou, Y. Cai, B. Zhang, J. Niu, S. Ji, S. Li, Appl. Catal. A 6180 (2002) 1.
[24] L. Chou, Y. Cai, B. Zhang, J. Niu, S. Ji, S. Li, React. Kinet. Catal. Lett. 76 (2002) 311.
[25] Z. Yu, X. Yang, J.H. Lunsford, M.P. Rosynek, J. Catal. 154 (1995) 163.
[26] D. Wang, M.P. Rosynek, J.H. Lunsford, J. Catal. 155 (1995) 390.
[27] E. Cordi, S. Pak, M.P. Rosynek, J.H. Lunsford, Appl. Catal. A 155 (1997) L1.
[28] J.H. Lunsford, E. Cordi, P. Qiu, M.P. Rosynek, Stud. Surf. Sci. Catal. 119 (1998) 227.
[29] S. Pak, J.H. Lunsford, Appl. Catal. A 168 (1998) 131.
[30] S. Pak, P. Qiu, J.H. Lunsford, J. Catal. 179 (1998) 222.
[31] A. Palermo, J.P.H. Vazquez, A.F. Lee, M.S. Tikhov, R.M. Lambert, J. Catal. 177 (1998) 259.
[32] A. Palermo, J.P.H. Vazquez, R.M. Lambert, Catal. Lett. 68 (2000) 191.
[33] A. Malekzadeh, A. Khodadadi, M. Abedini, M. Amini, A. Bahramian, A.K. Dalai, Catal. Commun. 2 (2001) 241.
[34] J.A. Sofranko, J.J. Leonard, C.A. Jones, J. Catal. 103 (1987) 302.
[35] C.A. Jones, J.J. Leonard, J.A. Sofranko, J. Catal. 103 (1987) 311.
[36] J.A. Sofranko, J.J. Leonard, C.A. Jones, A.M. Gaffney, H.P. Withers, Catal. Today 3 (1988) 127.
[37] J.A. Horsley, I.E. Wachs, J.M. Brown, G.H. Via, F.D. Hardcastle, J. Phys. Chem. 91 (1987) 4014.
[38] F. Kenn, R.A. Condrate Sr., J. Phys. Chem. Solids 40 (1979) 1145.
[39] F. Buciuman, F. Patcas, R. Craciun, D. Zahn, Phys. Chem. Chem. Phys. 1 (1999) 185.
[40] L.S. Bartell, K. Kuchitsu, R.J. de Neui, J. Chem. Phys. 35 (1961) 1211.